Sustainable Energy & Fuels

Nitro-oxidized Carboxylated Cellulose Nanofibers based Nanopaper and their PEM Fuel Cell Performance

Journal:	*Sustainable Energy & Fuels*
Manuscript ID	SE-ART-03-2022-000442.R1
Article Type:	Paper
Date Submitted by the Author:	13-Jun-2022
Complete List of Authors:	SHARMA, SUNIL KUMAR; Stony Brook University, Chemistry Sharma, Priyanka; Stony Brook University, Chemistry Wang, Likun; Stony Brook University, Pagels, Michael; Rensselaer Polytechnic Institute Borges, William; Stony Brook University , Chemistry Johnson, Ken; Stony Brook University Raut, Aniket; Stony Brook University, Material Science and Chemical Engineering Gu, Kevin; Stony Brook University, Bae, Chulsung; Rensselaer Polytechnic Institute, Chemistry and Chemical Biology Rafailovich, Miriam; Stony Brook University, Materials science and Engineering Hsiao, Benjamin; Stony Brook University, Department of Chemistry

Nitro-oxidized Carboxylated Cellulose Nanofibers based Nanopaper and their PEM Fuel Cell Performance

Sunil K. Sharma, *[1] Priyanka R. Sharma,[1] Likun Wang,[2] Micheal Pagel,[3] William Borges,[1] Ken I. Johnson,[1] Aniket Raut,[2] Kevin Gu,[1] Chulsung Bae,[3] Miriam Rafailovich,*[2] Benjamin S. Hsiao,*[1]

1.Department of Chemistry,
Stony Brook University, Stony Brook,
New York, 11794, United States

2. Department of Material Science and Chemical Engineering,
Stony Brook University, Stony Brook, New York, 11794, United States

3.Department of Chemistry and Chemical Biology,
Rensselaer Polytechnic Institute, Troy, New York, 12180, United States

Corresponding Authors:
SKS: Tel: +16314282528; E-mail: sunil.k.sharma@stonybrook.edu; MR: Tel:+15164589011; E-mail: miriam.rafailovich@stonybrook.edu; BSH: +Tel: +16316327793; E-mail: benjamin.hsiao@stonybrook.edu

ABSTRACT

The fuel cell is the best alternative to compensate for today's energy demand, but the high cost of fabrication of membrane (e.g., Nafion) hampers the prevalent commercialization. Plant-derived nanocellulose is a renewable, most abundant, and biocompatible with high strength and tunable surface chemistry. Here we have demonstrated the jute derived-Nitro-oxidized carboxycellulose nanofibers (NOCNF) as a viable and sustainable substitute for synthetic ionomer membrane used in proton exchange fuel cell (PEFC). NOCNF were obtained in two functionalities: carboxylate and carboxylic acid which then transformed into Nanopaper I and II, respectively. This is the first report where NOCNF with two different functionalities were tested in PEFC. The results indicated that Nanopaper II performed better than Nanopaper I with high proton conductivity of 14.2 mS cm^{-1} and power density of 19.1 mW cm^{-2} at high temperature (80º C) operation in PEFC, along with excellent durability even for 24 h of operation.

Keywords: Pant-based, Cellulose nanofibers, PEM fuel cell, Nitro-oxidation, Jute fibers

INTRODUCTION

The global population is projected to reach 9.7 billion by 2050, with this, the global electricity demand is expected to grow 150% to 53.6 billion MWh.[1] In order to sustainably meet this demand, improved energy efficient and renewable energy sources are needed. In this regard, hydrogen fuel cell technologies present an attractive energy carrying solution due to their flexibility, clean emissions, and efficiency.[2-8]

Proton exchange membrane fuel cells (PEMFC) are electrochemical devices that catalyze the spontaneous redox reaction between $H_{2(g)}$ and $O_{2(g)}$ to create a potential difference between electrodes.[9] Thus, energy from an intermittent source can be converted and used on demand from a gas-based storage. In particular, the only commercial proton exchange membrane used is Nafion, a fluoropolymer that conducts protons via sulfonic acid groups.[10, 11] Unfortunately, the limitations associated with Nafion include: (i) high cost i.e. ~US$ 800/m^2,[12], (ii) susceptibility to hydrogen gas crossover[13], (iii) complex recycling process[14], (iv) not biodegradable (V) loss of performance (proton conductivity and mechanical stability) at low relative humidity (RH) and high temperature[15]. Therefore, an inexpensive, greener, and more stable membrane is imperative to elevate the viability of PEMFC at large scale.

Plant-based nanocellulose is a most abundant, inexpensive and renewable nanomaterial that has potential in many different applications including pharmaceuticals,[16] food,[17] energy storage,[18] water purification,[19] biomedical,[20] 3D printing and tissue engineering.[21] Functionalized nanocellulose is one of the most anticipated alternative membrane precursors with several groundbreaking properties due to presence of abundant hydroxyl groups available for chemical

66 modifications or hydrogen bonding networks.[22-26] Mainly, there are two forms of plant derived
67 nanocelluloses: cellulose nanocrystals (CNC) and cellulose nanofibrils (CNF).[27] CNCs are
68 cellulose crystals with about 10 nm width and several hundreds of nanometers long; they are made
69 by strong acid hydrolysis of cellulose which removes more easily hydrolyzed noncrystalline
70 regions. [28] However, CNFs have varying morphologies than CNCs; they are mostly produced by
71 by TEMPO oxidation,[29-31] carboxymethylation,[32] phosphorylation,[33] acetylation,[34] silylation,[35]
72 nitro-oxidation[25, 27] on cellulose. Most of the above processes generate CNF with negative surface
73 charges which not only facilitate nanofiber dispersion in suspensions, but also provide functional
74 sites for utilization in various applications including adsorption, sensing, catalysis and for further
75 chemical modification.[36-43] Spherical shape nanocellulose has also been developed and
76 demonstrated to use in stabilizing the suspension of carbon nanotubes.[44-48]. The biopolymer based
77 nanocellulose-enabled membrane technology not only may be suitable for tackling global energy
78 challenges, but it can also provide a new low-cost platform for development of new energy storge
79 and generation technologies.[49]
80
81
82 CNF with high aspect ratio possess excellent mechanical properties such as Young's
83 modulus of 138 GPa and an estimated strength of 2-3 GPa.[50, 51] Additionally, the introduction of
84 carboxyl and sulfonic acid groups enable proton conduction through nanocellulose membranes.[52-
85 56] The fibrous morphology of CNF can be used to fabricate membranes with controlled pore sizes
86 that enable superior gas barrier properties comparable with Nafion.[57, 58] Beside that temperature
87 is also an important factor affecting the fuel cell performance. High temperature operation leads
88 to faster reaction kinetics, lower electrocatalyst loading, and improved water management, thereby

89 further can reduce the cost, however, higher temperature operation can put greater load on the
90 membrane.[9, 50, 59]

91

92 There are several previous studies of cellulose/ionomer composite membranes.[60-63] Gadim
93 et al. blended poly(4-styrene sulfonic acid) with bacterial cellulose and achieved an AC
94 conductivity of 14 mS cm^{-1} at 98% relative humidity (RH) and maximum power density of 40 mW
95 cm^{-2} at 125 mA cm^{-2}.[64] Jiang et al. made Nafion/bacterial nanocellulose composite membranes
96 which had a proton conductivity of 71 mS cm^{-1} and a power density of 106 mW cm^{-2} at 100% RH,
97 and at 30°C.[56] Notably, there are only few studies on functionalized nanocellulose membranes
98 (e.g. TEMPO oxidized, Sulfonated CNC) as the ionomer. Gadim et al. continued the study of
99 Nafion/nanocellulose blends and determined an in-plane proton conductivity to be 0.14 S cm^{-1} and
100 a maximum power density of 40 mW cm^{-2} at 125 mA cm^{-2} at 98% RH and room temperature.[64]
101 Hasani-Sadrabadi et al. made membranes with 5 wt% CNC and Nafion and observed a maximum
102 power density of 91 mW cm^{-2} at 70 °C in a direct methanol fuel cell, which was higher than pure
103 Nafion as there was reduced methanol crossover.[65] Finally, Tritt-Goc et al. created a high
104 temperature imidazole-doped CNC membrane that reached $2.7x10^{-2}$ S/m at 140 °C in dry
105 conditions.[66] Bayer et al. first reported the use of pure CNF and CNC membranes and found
106 superior gas barrier properties, but significantly lower conductivity of 0.01 mS cm^{-1} for CNF and
107 ~15 mS cm^{-1} for Nafion at 100% RH, and at 30 °C and power density of 0.79 mW cm^{-2} at 1.8 cm^{-2}
108 for CNF and ~450 mW cm^{-2} for Nafion.[13] The CNC membranes showed better performance but
109 they were brittle due to high crystallinity and can be cracked from heat pressing.[59] Hence, CNF
110 with high aspect ratio are required to maintain mechanical strength of membrane during the the
111 fuel cell operation.

In this work we have used simple one step Nitro-oxidation method which allows both resource and energy efficient production of carboxycellulose nanofibrils[27, 67] from jute-fibers with two different forms of carboxylate (COONa) and carboxylic (COOH) groups. Here the carboxycellulose nanofibril produced from Nitro-oxidation method are abbreviated as NOCNF. This is the first report where the presence of ionic (COO^-, carboxylate) and non-ionic (COOH, carboxylic) groups in the Nanopaper has been studied for their performance in PEMFC. It is hypothesized that the nanopaper having carboxylic group (COOH) will exhibit better performance in PEMFC because of the following facts: (i) carboxylic acid can accept and donate the proton, hence will act as a better charge carrier, (ii) it can exhibit more intense hydrogen bonding that can lead to more crosslinking resultant into denser and mechanically strong nanopaper which can be applicable for high temperature operation, (iii) carboxylic acid is hydrophilic that can lead to more water intake, hence can allow more proton transfer. Additionally, none of the report has demonstrated the use of cost-effective, less-chemically oriented pathway to design the ionomer membrane. We are the first to explore the NOCNF in preparation of such type of membranes useful in high tech applications (e.g., fuel cell).

EXPERIMENTAL SECTION

Untreated jute fibers (DP of extracted cellulose = 516) were provided by Toptrans Bangladesh Ltd. In Bangladesh. All samples were cut into small pieces having 3-5 cm in length and subsequently washed, but without further treatment. Analytical grade nitric acid (ACS reagent, 65%) and sodium nitrite (ACS reagent ≥ 97 %) were purchased from Sigma Aldrich; sodium bicarbonate, Hydrochloric Acid (37%) and HPLC grade DI water was purchased from Fisher

Scientific. All chemicals were used without further purification. Durapore membrane filter paper having a diameter of 47 mm and an average pore size of 0.1 μm was purchased from VWR.

Preparation of NOCNF

NOCNF were prepared by previously reported nitro-oxidation method.[25] In brief, 10 g dried jute fibers were placed in a 2 L three-neck round-bottom flask, where 140 mL of nitric acid (60%) was added. When the samples became completely mixed in the acid, 4.6 g of sodium nitrite was added to the reaction mixture under continuous stirring. The addition of sodium nitrite causes the generation of red gases inside the flask, which were prevented from escaping by closing the mouths of round-bottom flask with stoppers. The reaction was performed at 50 °C for 12 h and was then stopped by adding 500 mL of distilled water to the beaker. On equilibration of final reaction mixture, the supernatant liquid was discarded to remove the excess acid, leaving behind the fibers at the bottom. After doing the first decantation process, a mixture of ethanol and water (1:2 ratio) was added to the fibers, and then the suspension was stirred. The sample was kept untouched until the liquid (supernatant) and solid fibers became separate layers. The supernatant was also decanted off to extract the fibers. The above decantation step was repeated 4−5 times, until the pH value of fiber suspension reached above 2.5. This suspension was then transferred into a dialysis bag for 4−5 days until the conductivity of water reached below 5 μS. Once the dialysis of fiber suspension gets finished the fibers were then treated with sodium bicarbonate (8 wt % sodium bicarbonates) to obtain a good dispersion, so that it can easily homogenized to obtain the nanofibers suspension. Hence, the fibers were then passed to a high-pressure homogenizer (GEA Niro Soavi Panda Plus Bench top homogenizer) at 250 bar for 1 cycle. The obtained nanofibers

were again dialyzed (using a dialysis bag, Spectral/Por; with MWCO: 6−8 kDa) and equilibrated for 2−4 days, until the conductivity of water reached below 5 μS. The obtained nanofibers possessed the carboxylate groups (COO^-Na^+) and termed as CNF-Na.

One portion of above nanofibers was then treated with 0.1 M Hydrochloric acid until pH of suspension reach to 2 and dialyzed for conversion of -COONa functionality to -COOH. This nanofiber suspension was named as CNF-H. The schematic diagram on preparation of CNF-H and CNF-Na with two different functionalities using the nitro-oxidation approach is shown in Figure 1.

Preparation of Nanopaper

Nanocellulose suspension in water (CNF-Na and CNF-H) with 0.20 wt% concentration and volume 200 mL were stirred separately for 3 h at 320 rpm to make the suspension homogenous. Then the suspension of these CNF vacuum filtered by using microfiltration assembly composed of a glass support Ultra-Ware glass funnel connected to a vacuum pump, where the funnel was fitted with a Durapore membrane filter paper having a diameter of 47 mm and an average pore size of 0.1 μm. The aggregation of the nanofibers (CNF-H and CNF-Na) layer was formed continuously on top of the membrane paper until a uniform wet sheet of nanopaper was achieved. The wet nanopaper sheet was then removed from the membrane paper, and placed between two Kapton films and hot-pressed at 110 °C for 20 min. To avoid the wrinkling of the nanopaper edges, the resulting nanopaper was compressed under 2 kg of weight at room temperature for 10 h. The nanopaper prepared using CNF-Na suspension was termed as Nanopaper I while nanopaper II

developed using CNF-H suspension was named as Nanopaper II. The thicknesses of the Nanopaper I and Nanopaper II were in the range of 60-62 μm.

XPS Analysis

The O1s peak was calibrated to 532 eV and C1s peak to 284.8 eV.

Proton Conductivity

In-plane ion conductivity measurements were determined using a Scribner 740MTS instrument for temperature and humidity control (under N_2 atmosphere). Using a four-point probe, impedance was measured with an AC amplitude of 10 mV in a frequency range from 10 Hz to 10^5 Hz. Measurements were taken at 100% RH and at 30, 45, 60 and 80 °C. The samples were equilibrated to the appropriate testing conditions for 0.5 h prior to the impedance measurement. Resistance was determined from the high frequency x-intercept of the semicircle of Nyquist plots. Conductivity was calculated from the following equation:

$$\sigma = \frac{L}{A * R} \qquad \text{Eq. 1}$$

Where σ is the calculated conductivity, L is the length between the two inner probes, A is the cross-sectional area of the membrane and R is the resistance.

Fuel Cell Performance

The 5 cm^2 membrane electrode assembly (MEA) was made by hot-pressing the two commercial carbon cloth electrodes (0.1mg/cm^2 Pt loading, Fuel Cell Etc.) onto the opposing sides of Nanopapers under the condition of 2 MPa at 140 ^oC for 1 min after waiting 5 min for temperature to stabilize. The single cell performance was evaluated on a fuel cell test station (Fuel Cell Technology). The anode and cathode were fed with humidified H_2 and O_2 at 80 ^oC with 100% RH. H_2/O_2 gas fluxes were both controlled at 100 cm^3/min and externally humidified at the dew point temperature. The performance test was conducted after 1h humidification. The backpressure for both the anode and cathode was varied from 0, 8 and 21 psi for the collection of polarization and power curves.

RESULTS AND DISCUSSION

Characterization of NOCNF (CNF-H and CNF-Na)

The nitro-oxidation approach was designed to treat raw biomass, especially nonwood biomass, aiming to make the nanofibers extraction more facile, more sustainable, less chemical oriented, and less energy dependent. Based on our previous nitro-oxidation study the primary factor affecting the morphology and surface charge of NOCNF was the amount and concentration of nitric acid used.[25, 27] However, the decrease in nitric acid concentration to 60% could result in high aspect ratio NOCNF having a significant portion of fiber length without changing the average width.[68] Typically, when CNF has a good aspect ratio and high surface charge, the suspension can result in a homogeneous gel.[69] The CNF-Na sample obtained in the current study possess the surface charge of -117 mV in the form of COONa with concentration of 0.94 mmol/g.

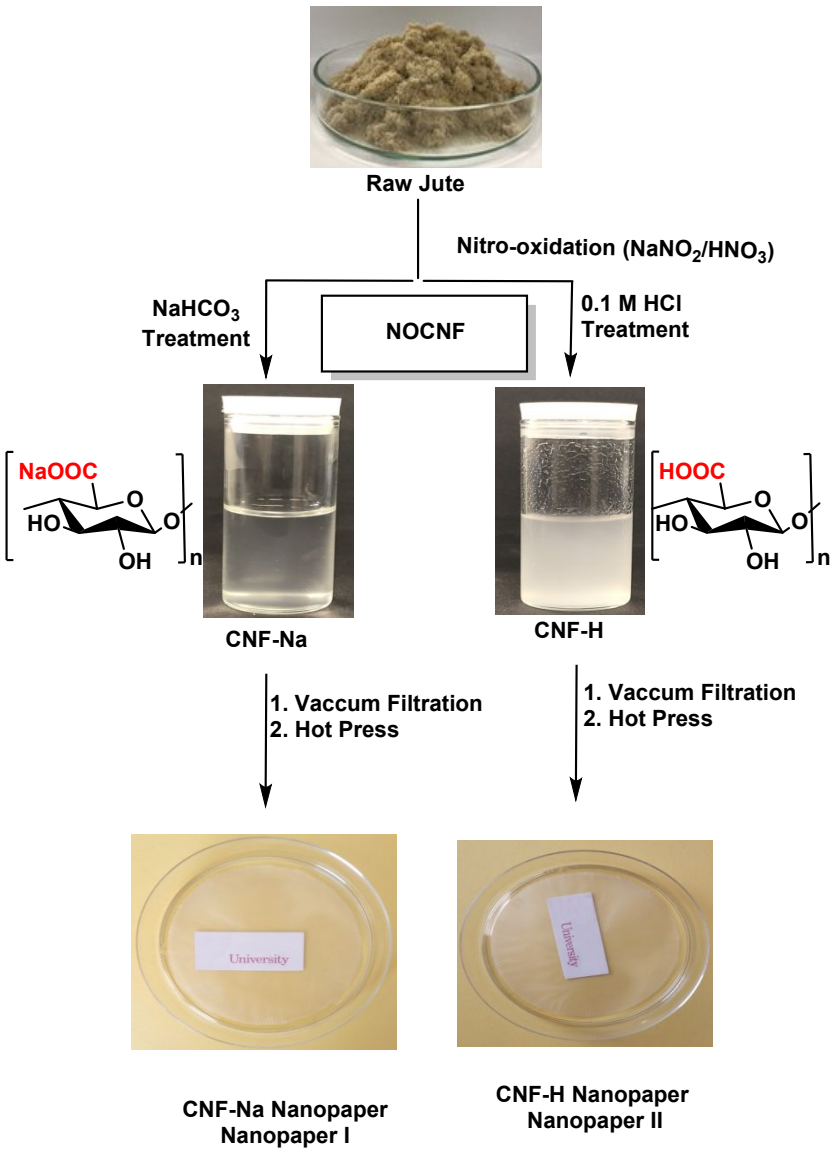

Figure 1. Schematic preparation of Nanopapers from raw jute fibers: Nanopaper I and Nanopaper II prepared by using CNF-Na and CNF-H respectively.

Further -COONa group of nanofibers were converted to –COOH group to introduce highly acidic protons by treating CNF-Na suspension with 0.1 M HCl until the pH of suspension reach to 2 followed by dialysis. The surface charge for these CNF-H nanofibers was found −72 mV. This

indicates that this acidic treatment has led to a partial conversion of ionic -COO^-Na^+ groups to nonionic -COOH forms in CNF-H.

Figure 2 (i & ii) presents the TEM image of CNF-H and CNF-Na samples. The average length and width measured for CNF-Na was 511±151 and 7.6±1.9 nm. While the average length and width obtained for CNF-H was 338±127 and 7.7±1.8 nm. The results indicate the decrease in the length of fibers on acidic treatment without change the fibers width. It is obvious that the acidic treatment of cellulosic fibers can cause the degradation of fiber by breakage of 1,4-glycosidic bonds in cellulose chains.[45]

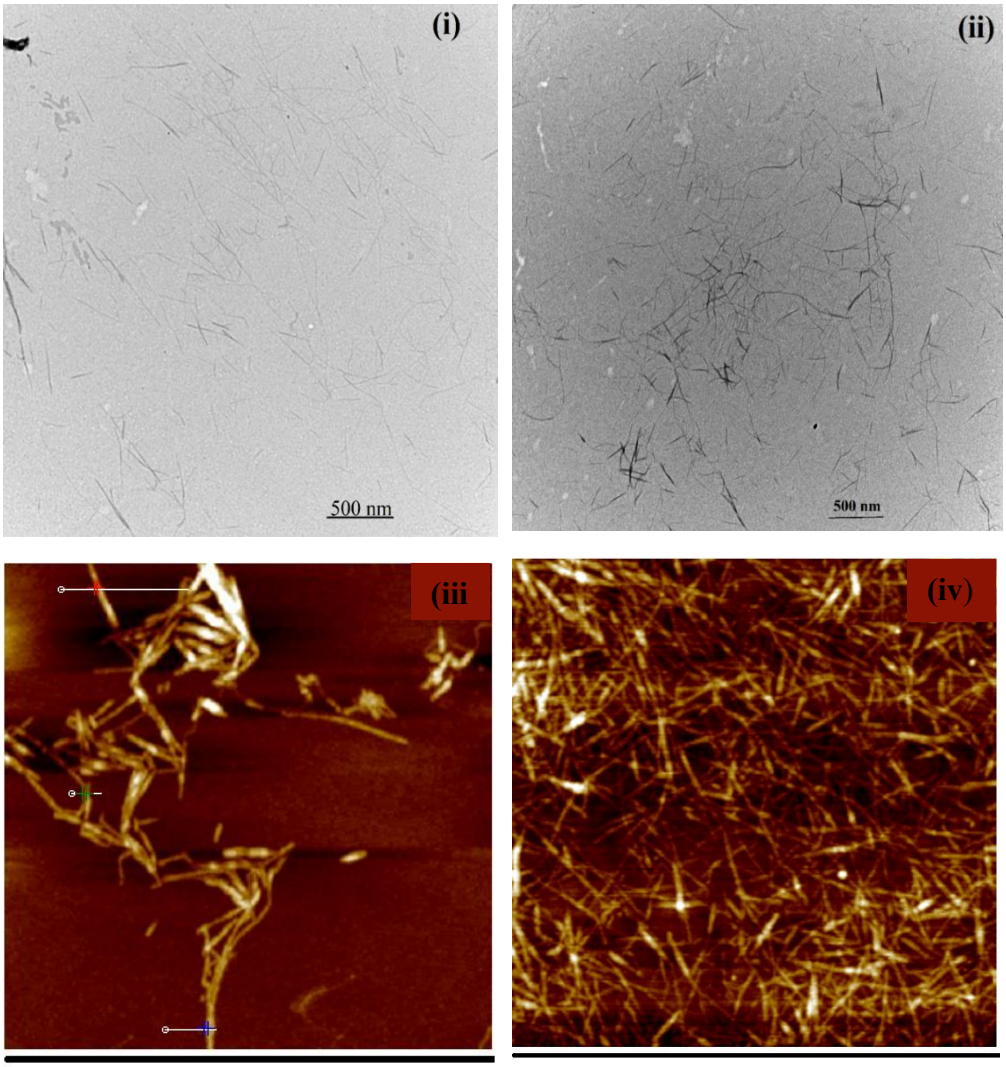

Figure 2. TEM image of NOCNF extracted from jute (i) CNF-Na (ii) CNF-H (taken at scale bar of 500 nm and magnification of 329,0000X); AFM images of NOCNF (iii) CNF-H (iv) CNF-Na taken at 2.5 μm scale.

The AFM images of CNF-Na and CNF-H are presented in Figure 2(iii & iv). It is observed that CNF-Na (Figure 2(iii)) has not shown any aggregations of nanofibers. While CNF-H has presented strong accretion behavior likely due the additional hydrogen bonding interaction between the cellulose chains resulted from COOH groups.[70] The photographs of CNF-Na and CNF-H suspension is shown in Figure 1 further provide the evidence of accretion behavior in CNF-H. It is observed that CNF-Na suspension is clearer and more transparent, however CNF-H suspension is nontransparent.

Surface Functionality, Chemical Composition and Thermal Properties of Nanopaprs

The surface functionality of Nanopaper I and II prepared from NOCNF suspension was first carried out by FTIR. The FTIR spectra of both Nanopapers are presented in Figure 3 (i). In these spectra, the dominant 3328 cm^{-1} peak due to the OH stretching and the weaker 2900 cm^{-1} peak due to the -CH symmetrical stretching (all from the cellulose component) was present in both Nanopaper samples. The sharp peak appears around 1515 cm^{-1} in both Nanopapers is due to C=C aromatic symmetrical stretching in the lignin unit, while peaks appear at 1739, 1460, 1240, and 810 cm^{-1} in the xylan and glucomannan of hemicellulose units.

The appearance of a sharp 1602 cm^{-1} peak in Nanopaper I confirmed the presence of C=O group of COONa functionality; while a sharp C=O absorption band at 1720 cm^{-1} is assigned to C=O stretching of COOH functionality in Nanopaper II.[70]

The thermogravimetric and derivative thermogravimetric analysis of Nanopaper I and II is shown in Figure 3(ii). The thermal degradation profile of both the Nanopapers exhibited almost similar and two major degradation steps, whereby the initial onset temperature (T_{onset}) was at 200°C with 8.2 wt % weight loss, and the final offset temperature (Toffset) was at 305 °C with 48 wt % weight loss. The shifting of the T_{onset} value to a lower temperature of Nanopapers (Nanoaper I and II) as compared to that of raw biomass indicates the lower thermal stability of these Nanopapers might be due to the presence of thermally unstable anhydroglucoronic moiety in nanofibers, which could be degraded at a lower temperature (~200 °C) and release CO_2.[48] The major difference in the TGA profile of Nanopaper I and II is the amount of residual weight obtained at 550 °C. In case of Nanopaper I the residual weight was around 16.38%, while in the case of Nanopaper II it was 12.49%. The higher residual weight % in the case of Nanopaper I can be explained by the presence of residual metal oxide resulted from the thermal decomposition of COONa functionality.

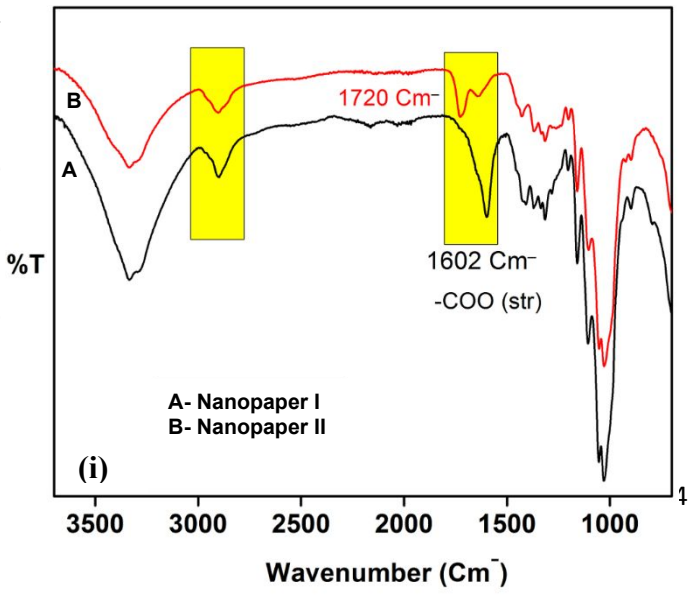

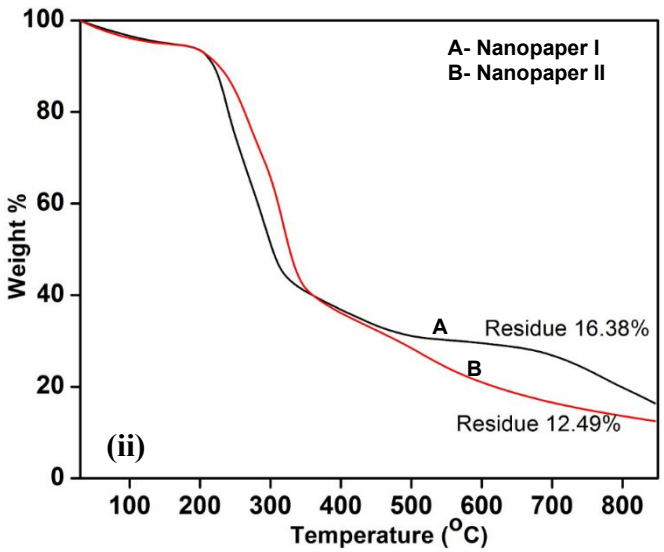

Figure 3. (i) FTIR spectra of Nanopaper I and II; (ii) TGA curves of Nanopaper I and II.

Figure 4(i) shows the XPS wide scan of Nanopaper I and II. The Na KLL Auger peak was observed at 497 eV in Nanopaper I. Using the sensitivity factor for C1s and O1s of 1.00 and 2.93 respectively, the elemental composition of Nanopaper I was calculated to 62.4% carbon and 34.3% oxygen. The elemental composition of Nanopaper II was calculated to 67.2% carbon and 32.4% oxygen. The C1s peak of both the Nanopapers can be deconvoluted into four smaller peaks. Fitting was done using a Shirley background, Gaussian curve fitting, and constraining peak position, area, and full width at half maximum (FWHM). From greatest to lowest relative area shown in Figure 4(ii), the C-C, C-H peak corresponded to the cellulose backbone ring and hydrocarbon bonding. The C-OH is attributed to carbon bonded alcohol groups in the cellulose chain. The O-C-O peak appeared due to acetal groups. While the O=C-O peak is from carboxyl groups. The O1s peak of Nanopaper I and II was deconvoluted to four peaks shown in Figure 4(iii). The O=C-O peak corresponded to carbonyl oxygen of the acid, C-OH is attributed to the alcohol group, C-O-C-O resulted from the acetal group and O-C=O was assigned to singly bonded oxygen of the acid. On Comparing XPS spectra of both Nanopapers in Figure 4(iii), the O-C=O and O=C-O contribution was estimated approximately equally to be in agreement to the theoretical structure of carboxylated cellulose. Moreover, the largest contribution was from the C-OH bond (~40%) which confirms not all alcohols of cellulose were oxidized, likely secondary alcohol groups remained. Fitting for the carboxylic acid of both C1s and O1s was based on the carboxylate content calculated from

conductometric titration; 0.94 mmol of carboxylate per gram of cellulose. Because cellulose has a structure of $C_6H_{10}O_5$, it is estimated that six out of every twenty-one atoms are carbon. And for every mol of carboxylate, there is one mol of carbon. On these assumptions, we estimated the C1s O=C-O contribution to 3.9%. A similar estimate was done for each oxygen of the O1s O=C-O, while also constraining the peak areas to be equal during fitting.[71]

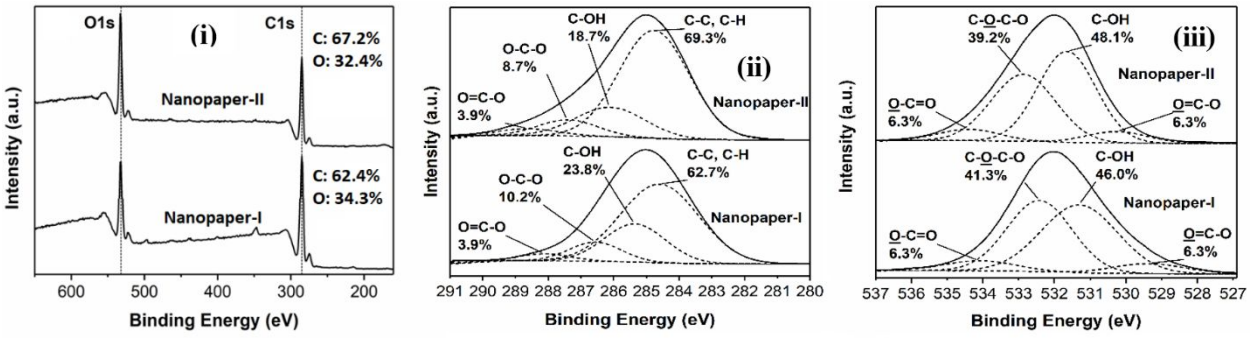

Figure 4. (i) XPS wide scan spectra of Nanopaper I and II and elemental composition. (ii) Deconvoluted C1s spectra of Nanopaper I and II with relative bond distribution. (iii) Deconvoluted O1s spectra of Nanopaper I and II with relative bond distribution.

The contact angle measurement for Nanopaper I and II is presented in Figure S1 (*Supporting Information*). The average contact angle observed for Nanopaper I and Nanopaper II was 47.2^o and 34.4^o respectively. Lower contact angle value for Nanopaper II indicates more hydrophilicity as compared to Nanopaper I showed high water intake capability of Nanopaper II. This further confirms the presence of highly acidic and hydrophilic COOH groups on the surface of Nanopaper II.[72]

WAXD measurements were carried out as shown in figure 5(i) to confirm the crystallinity index as well as the crystal structure of Nanopapers. The WAXD patterns of Nanopapers indicate that both the Nanopapers have exhibited cellulose I structure with diffraction peaks at 2θ angles of 16.5°, 22.7°, and 35.1° corresponding to (110), (200), and (004) reflections, respectively. This further provides the evidence of change of COONa to COOH functionality in NOCNF did not change the crystal structure of cellulose chain. The crystallinity index (CI) calculated from the WAXD data for Nanopaper I was 77%, while that for Nanopaper II was 60.9 %. The lower crystallinity of Nanopaper II could be because of the additional acid treatment that has employed to convert the COONa groups in NOCNF to COOH.

Solid state ^{13}C CPMAS NMR spectra of Nanopaper I and Nanopaper II are shown in Figure 5(ii). The NMR spectra of both the Nanopaper shows the distinct peaks of cellulose I chain as follows: (i) peaks between 60-70 ppm belong to C6 carbon of the primary alcohol group, (ii) a group of peaks in between 70-80 ppm attributed to the C2, C3, and C5 carbons, (iii) peak between 80-95 ppm associated with C4 carbon, (iv) peaks between 100-110 ppm was due to the anomeric carbon C1.[58] Most importantly, the peak corresponds to carboxylate carbon for Nanopaper I appeared at 178 ppm while for Nanopaper II, it shifted more downfield at 172 ppm. This is because Nanopaper I consist of COONa groups where Na^+ ions are more electropositive than H^+ of COOH in Nanopaper II.

Tensile properties of two Nanopaper I and II are shown in Figure 5(iii). The Nanopaper I prepared by CNF-Na whose average L and W was 511±151 and 7.6±1.9 nm, respectively. While the Nanopaper II prepared by using CNF-H showed the average L and W in the range of 338±127

and 7.7±1.8 nm respectively. Hence, the Nanopaper I exhibited higher aspect ratio (L/D) of 67.2 as compared to aspect ratio of Nanopaper II which was 43.8. The higher aspect ratio for Nanopaper II should led to excellent mechanical properties.[69] However, in this study we have observed opposite trend where Nanopaper I comprised of high aspect ratio CNF-Na showed lower tensile strength of 89±1.2 MPa at elongation at break ratio of 2.2 ±0.2%, while Nanopaper II consist of low aspect ratio CNF-H exhibited high tensile strength of 112±2 MPa with elongation at break ratio of 3.0 ± 0.2%. The most probable reason for this opposite trend could be the presence of COOH groups in Nanopaper II that has induced strong hydrogen bonding owing to its strong tensile strength.

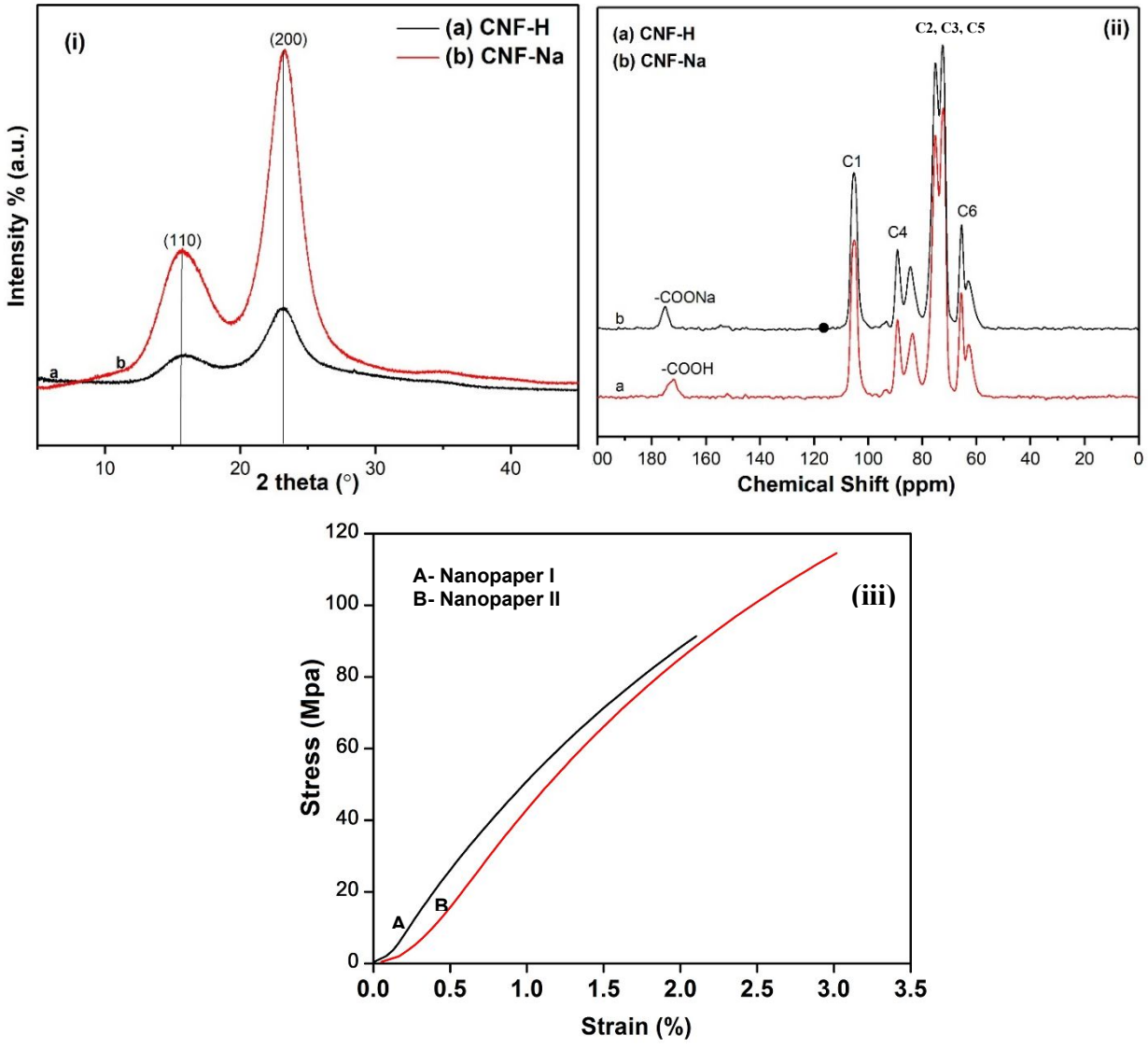

Figure 5. (i) WAXD patterns of Nanopaper I and II. (ii) ^{13}C CPMAS NMR spectra of Nanopaper I and II. (iii) Tensile curves for Nanopaper I and II.

Surface Morphology, BET Surface area, Mechanical Properties of Nanopapers

Photographs of two nanocellulose suspensions (CNF-Na and CNF-H) and their corresponding Nanopaper I and II are shown in Figure 1. Suspension of CNF-Na looks clear and highly suspended due to presence of ionic -COONa groups, while CNF-H suspension appearances more blurred likely due to aggregation of nanofibers via hydrogen bonding induce by their -COOH groups. Similarly, the Nanopaper I looks more transparent than Nanopaper II.

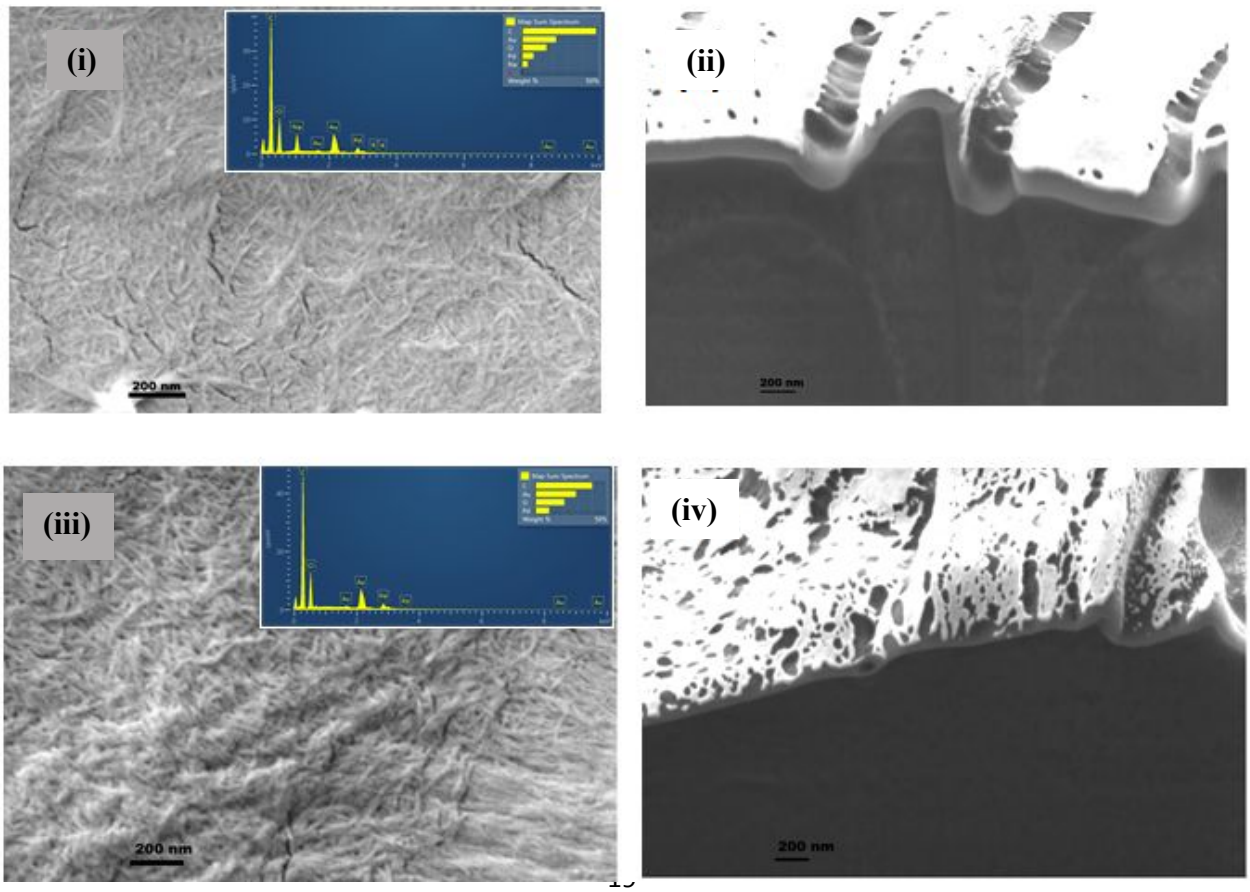

436

437

438 **Figure 6**. (i) SEM image and EDX elemental mapping for Nanopaper I (ii) SEM image of cross
439 section of Nanopaper I (iii) SEM image and EDX elemental mapping for Nanopaper II (iv) SEM
440 image of cross-section of Nanopaper II.

441

442 SEM images in Figure 6 present exterior and interior morphology of Nanopaper I and II.
443 Both the Nanopapers consists of a network of randomly interwoven fibers. The surface of
444 Nanopaper I looks smooth with evenly distributed fibers. While surface of Nanopaper II appeared
445 rough likely due highly crosslinked hydrogen bonded fibers by COOH functional groups as
446 discussed in FTIR section. The difference between surface morphologies of both the Nanopapers
447 is quite depictive in their respective cross-section SEM images. The cross-section SEM image of
448 Nanopaper I shows with big pores along with few small tinny pores on the smooth surface, while
449 on the surface of Nanopaper II more evenly distributed pores were observed which are smaller in
450 the size compared to Nanopaper I, which further evidence that Nanopaper II comprised of highly
451 crosslinked and interconnected fibers resultant into its smooth and denser membrane.

452

453 The BET measurement for Nanopaper I and Nanopaper II is presented in Figure S2 in
454 *Supplementary Information*. The measured surface area for Nanopaper I and II was 1.83 and 0.87
455 m^2/g respectively. The lower surface area value for Nanopaper II compared to Nanopaper I
456 indicates that Nanopaper II structure is comparatively denser due to highly crosslinked nanofiber
457 network which is clearly seen in SEM image of Nanopaper II. Both the Nanopapers I and II
458 possessed very small total mesopore volumes of 0.006 and 0.002 cc g^{-1}, respectively (presented in

Figure S3 in *Supplementary Information*). The low pore volume indicates the good gas barrier properties of both Nanopapers I and II, and allow them suitable for hydrogen fuel cell applications.[59]

Fuel Cell performance

Till now functionalized nanocellulose membrane with COOH functionality in PEMFC has not been reported in the literature to the best of our knowledge. Both the Nanopapers has shown excellent performance as a proton conducting electrolyte and contributed to the performance of the assembled fuel cell. Additionally, the effect of back pressure was studied. The high backpressure has enhanced the power output of the MEA in both cases. For example: Nanopaper I and II exhibited the open circuit voltage (OCV) of 0.70 and 0.85 V respectively, while OCV for the commercial membrane based fuel cells such as Nafion found 0.94 V when measured under similar conditions.[6] This confirms that the NOCNF Nanopaper based paper electrolyte works competently in transporting protons and blocking electrons while maintaining a very low hydrogen crossover. The probable reason for Nanopapers to demonstrate such properties is their dense and cross-linked surface topography caused by their surface functionalities (COOH and COONa).

Figure 7(i and ii) shows the polarization curves for Nanopaper I and II. The OCV found for Nanopaper I was 0.70 V which immediately dropped to 0.60 V on increasing current, this type of behavior exhibits its activation losses during the operation. Similar trend has been reported in commercial Nafion membrane.[15] In the case of Nanopaper I, a maximum power density of 1.8 mW cm^{-2} at a current density of 4.1 mA cm^{-2} was achieved when 8 psi of back pressure was applied.

A significant increment in current density to 8.9 mA cm^{-2} was observed when back pressure increased to 21 psi. Notably, no OCV and power generation was observed in Nanopaper I at 0 back pressure which is likely due to its low proton conductance and higher resistance which is discussed later in proton conduction section.

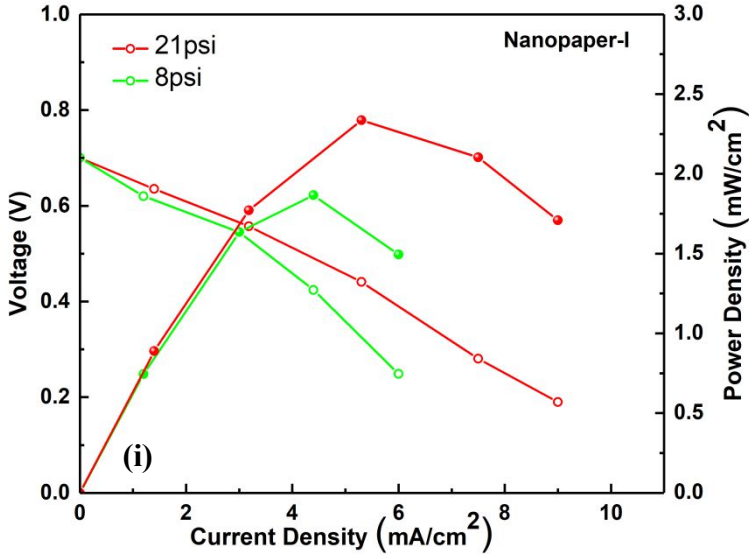

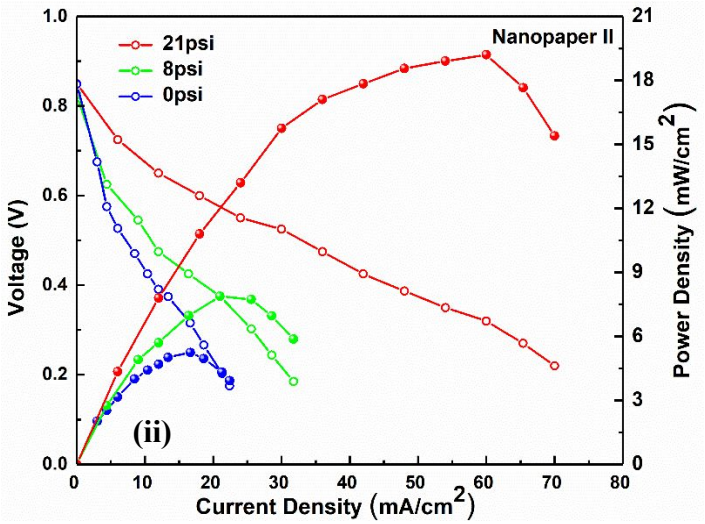

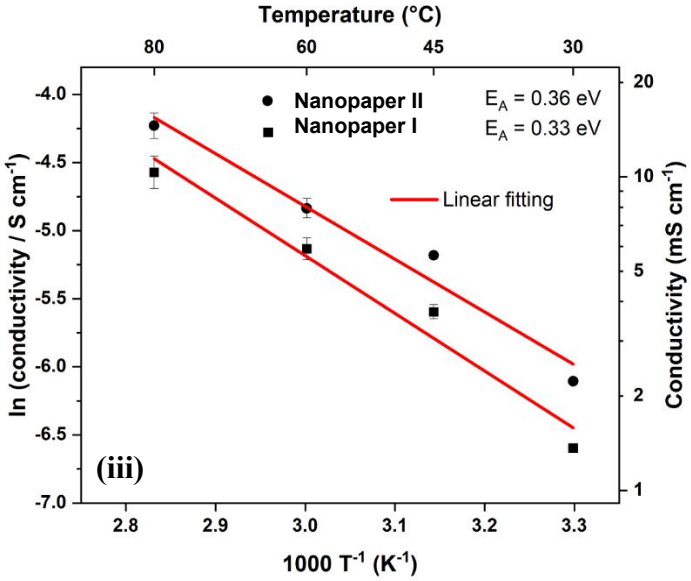

Figure 7. Polarization and power curves for (i) Nanopaper I (ii) Nanopaper II under various oxygen pressure conditions; (iii) Arrhenius plot of the conductivity of the Nanopaper I and II (at 100% RH) with activation energies.

For Nanopaper II, three polarization curves were obtained at three different back pressures of 0, 8, 21 psi at operating temperature of 80 ^{o}C which is shown in Figure 7(ii). In the case of Nanopaper-II OCV measured was 0.87 V which is higher compared to Nanopaper I. The increased OCV was due to more strength and high proton conduction due to presence of highly acidic COOH groups on the surface of the nanofibers in Nanopaper II, while Nanopaper I comprised of COONa groups. The OCV for Nanopaper II remained constant at 0.87 V at all three back pressures of 0, 8 and 21 psi used during the experiments. It showed maximum power densities of 4.1, 6.2 and 19.2 mW cm^{-2} when 0, 8 and 21 psi back pressure were applied, respectively. Highest power density of 19.1 mW cm^{-2} at a current density of 57.2 mA cm^{-2} was achieved for Nanopaper II, when 21 psi of back pressure was applied. This is about 5 times higher than the power density achieved at 0 psi back pressure and 3 times higher than the power density attained at 8 psi. Additionally, the maximum current density observed for Nanopaper II is about 10 times higher than maximum current density observed for Nanopaper I. The overall results indicate that the Nanopaper II shows better conductance comparison to Nanopaper I. This could be because of following reasons: (i) the presence of highly acidic -COOH groups on the surface of Nanopaper II has aided to better proton transfer, (ii) the uniform and highly dense surface in Nanopaper II occurred by high degree of crosslinking from -COOH groups may have accounted in preventing hydrogen gas oozing through the membrane while allowing proton migration, which resultant into a higher performance (e.g.,

high OCV).[59] These results fully support our hypothesis of using COOH functionalized nanopaper in PEMFC.

The high backpressure has led to high power output of the MEA in both cases which is likely due to decrease in cell ability to drain out water because of enhanced RH in cathode channel on applying high back pressure leading to high membrane water content which aids to improvement in the PEMFC performance.[73] However, the OCV of Nanopaper II cell remained around 0.87 V regardless of the variation in back pressure (Figure 7 (ii)) which is 100 mV higher than the Nanopaper I based fuel cell. Notably, the fuel cell performance for Nanopaper II is significantly higher than the similar TEMPO oxidized nanofiber membrane system reported previously in the literature.[13] TEMPO oxidized nanofibers based membrane possessed COONa functionality[13] like Nanopaper I. In summary, in this study we have proven that the functionality changes of COONa in Nanopaper I to COOH in Nanopaper II has tremendously improved the performance of the MEA.

A durability measurement was performed on Nanopaper II based fuel cell at 80 °C under constant current of 11 mA and initial voltage of 0.6 V for 24 h presented in Figure S4 in *Supporting Information*. Only a slight cell voltage fluctuation by ±0.5 V was observed. This fluctuation could be the result of small pressure variations generally occurred during the operation. Overall, this measurement confirms the steady operation of Nanopaper II fuel cell at 80 °C and provide a new insight to substitute the synthetic membrane with a sustainable and cost-effective high-temperature Nanopaper membrane in the operation of PEMFCs.

549 The slop of Arrhenius plot can be used to determine the activation energy (E_A) which can
550 provide vital information about the possible mechanism for the proton transportation. High proton
551 conductivity of membranes plays an important role in decreasing ohmic resistance and in
552 increasing cell performance in a fuel cell.[74] Nanopaper I and II were tested at 100 % RH to
553 investigate their proton conduction mechanism. Figure 7(iii) displays the Arrhenius plot of the
554 conductivity for both Nanopapers measured under variable operating temperatures of 30, 45, 60
555 and 80 ˚C. It was observed that with increase in temperature from 30 to 80 °C, the conductivity of
556 Nanopaper I and II increased from 1.4 to 10.4 mS cm^{-1} and from 2.2 to 14.6 mS cm^{-1}, respectively.
557 The slope from a linear fit of the data points allows E_A of proton conduction to be calculated. In
558 the literature, two mechanisms: vehicular and Grotthuss have been described to explain the proton
559 transport in humidified conditions through the membrane.[59] The vehicular mechanism involves
560 the transport of a charge by hydronium ion that generally owe to higher E_A. While Grotthus
561 mechanism describes the transport of proton through the bonding and de-bonding in a hydrogen
562 bonded network, hence leads to low E_A. In present study, Nanopaper I and II have shown E_A of
563 0.36 and 0.33 eV, respectively. While the Nanopaper from CNC and TEMPO oxidized nanofibers
564 reported earlier have shown E_A of 0.21 and 0.24 eV [13] and Nafion shows E_A of 0.16 eV Nafion
565 follows Grotthus like proton transport where it supports proton transport through a complete
566 hydrogen bonding network.[13] The E_A measurements indicate that Nanopaper II has better hydrogen
567 bonded ion conduction networks causing more facile proton conduction because of the presence
568 of COOH functionality. The above results indicate that NOCNF based Nanopaper are viable and
569 sustainable development for PEM fuel cell. As described, the Nanopapers used in this study are
570 derived from NOCNF which is extracted using Nitro-oxidation method. Nitro-oxidation is highly
571 efficient in generating negative surface charge on fibers which owe to nanofibers with ample

amount of polyelectrolyte polymeric chains having COOH groups. This way NOCNF offer alternatives to synthetic PEM fuel cell membranes (e.g., Nafion) for membrane design.

Conclusions

Plant-based nanocellulose were extracted from jute fibers using simple, cost-effective and less chemically oriented pathway 'Nitro-oxidation' approach and further two Nanopapers with different functionalities of COONa (Nanopaper I) and COOH (Nanopaper II) were fabricated. These Nanopapers displayed proton conductivity that is highly dependent on surface functionality and temperature. Among two Nanopapers, the Nanopaper II has presented better proton conduction and fuel cell performance. This is attributed to highly acidic -COOH groups which has not only served as a proton donor/charge carrier but also provided dense and strong structure to Nanopaper through crosslinking of nanofibers by numerous hydrogen bonding interactions. The maximum conductivity observed for Nanopaper II was 14.6 mS cm^{-1} at 80 °C (at 100% RH). The higher conductivity in Nanopaper II even at high temperature (80 °C) is ascribed to COOH groups introduced during the nitro-oxidation that acted as a charge carrier. Fuel cells utilizing NOCNF Nanopapers were fabricated and tested at 80 °C and 100% RH using hydrogen fuel. As expected, because of the higher conductivity, dense surface, hydrophilicity and tensile strength, fuel cells incorporating Nanopaper II displayed good performance with power density of 19.1 mW cm^{-2} than Nanopaper I which has exhibited power density of 5.8 mA cm^{-2}. Durability test on Nanopaper II confirms its stability in fuel cell operation at 80 °C for 24 h. These results show that nitro-oxidized nanocellulose paper can be applied as a sustainable, environment-friendly, and

inexpensive source to fabricate the high-temperature ionomer membranes useful in electrochemical devices (e.g., fuel cell).

Acknowledgement

The authors acknowledge financial support from the Polymer Program of the Division of Materials Research in the National Science Foundation (DMR-1808690). The authors would like to thank Dr. Jim Quinn (Materials Science and Engineering- Stony Brook University) for SEM analysis, Tomas Rosen (Stony Brook University) for helping in TOC image and Dr. Chung-Chueh Chang (ThINc-Stony Brook University) for TGA, TEM and AFM analysis.

References

1. WHO, *https://www.un.org/en/development/desa/news/population/2015-report.html*, 2015, Retrived 24 June, 2020.
2. M. Winter and R. J. Brodd, *Chemical Reviews*, 2004, **104**, 4245-4270.
3. C.-Y. Wang, *Chemical Reviews*, 2004, **104**, 4727-4766.
4. P. P. Edwards, V. L. Kuznetsov, W. I. F. David and N. P. Brandon, *Energy Policy*, 2008, **36**, 4356-4362.
5. I. Staffell, D. Scamman, A. Velazquez Abad, P. Balcombe, P. E. Dodds, P. Ekins, N. Shah and K. R. Ward, *Energy & Environmental Science*, 2019, **12**, 463-491.
6. L. Wang, S. Bliznakov, R. Isseroff, Y. Zhou, X. Zuo, A. Raut, W. Wang, M. Cuiffo, T. Kim and M. H. Rafailovich, *Applied Energy*, 2020, **261**, 114277.
7. X. Xiao, H.-q. Xia, R. Wu, L. Bai, L. Yan, E. Magner, S. Cosnier, E. Lojou, Z. Zhu and A. Liu, *Chemical Reviews*, 2019, **119**, 9509-9558.
8. K. V. Kordesch and G. R. Simader, *Chemical Reviews*, 1995, **95**, 191-207.
9. L. Wang, X. Zuo, A. Raut, R. Isseroff, Y. Xue, Y. Zhou, B. Sandhu, T. Schein, T. Zeliznyak, P. Sharma, S. Sharma, B. S. Hsiao and M. H. Rafailovich, *Sustainable Energy & Fuels*, 2019, **3**, 2725-2732.
10. K. A. Mauritz and R. B. Moore, *Chemical Reviews*, 2004, **104**, 4535-4586.
11. P. Sapkota, C. Boyer, R. Dutta, C. Cazorla and K.-F. Aguey-Zinsou, *Sustainable Energy & Fuels*, 2020, **4**, 439-468.
12. T. Wilberforce, A. Alaswad, A. Palumbo, M. Dassisti and A. G. Olabi, *International Journal of Hydrogen Energy*, 2016, **41**, 16509-16522.
13. T. Bayer, B. V. Cunning, R. Selyanchyn, M. Nishihara, S. Fujikawa, K. Sasaki and S. M. Lyth, *Chemistry of Materials*, 2016, **28**, 4805-4814.
14. R. S. L. Yee, R. A. Rozendal, K. Zhang and B. P. Ladewig, *Chemical Engineering Research and Design*, 2012, **90**, 950-959.

15. A. K. Sahu, S. Pitchumani, P. Sridhar and A. K. Shukla, *Bulletin of Materials Science*, 2009, **32**, 285-294.
16. S. Salimi, R. Sotudeh-Gharebagh, R. Zarghami, S. Y. Chan and K. H. Yuen, *ACS Sustainable Chemistry & Engineering*, 2019, **7**, 15800-15827.
17. H. M. C. Azeredo, M. F. Rosa and L. H. C. Mattoso, *Industrial Crops and Products*, 2017, **97**, 664-671.
18. B. Thomas, M. C. Raj, A. K. B, R. M. H, J. Joy, A. Moores, G. L. Drisko and C. Sanchez, *Chemical Reviews*, 2018, **118**, 11575-11625.
19. P. R. Sharma, S. K. Sharma, T. Lindström and B. S. Hsiao, 2020, **4**, 1900114.
20. P. R. Sharma, S. K. Sharma, T. Lindström and B. S. Hsiao, *Advanced Sustainable Systems*, 2020, **4**, 1900114.
21. D. Klemm, E. D. Cranston, D. Fischer, M. Gama, S. A. Kedzior, D. Kralisch, F. Kramer, T. Kondo, T. Lindström, S. Nietzsche, K. Petzold-Welcke and F. Rauchfuß, *Materials Today*, 2018, **21**, 720-748.
22. P. R. Sharma, S. K. Sharma, R. Antoine and B. S. Hsiao, *ACS Sustainable Chemistry & Engineering*, 2019, **7**, 6140-6151.
23. H. Chen, S. K. Sharma, P. R. Sharma, H. Yeh, K. Johnson and B. S. Hsiao, *ACS Omega*, 2019, **4**, 22008-22020.
24. C. Zhan, Y. Li, P. R. Sharma, H. He, S. K. Sharma, R. Wang and B. S. Hsiao, *RSC Advances*, 2019, **9**, 40565-40576.
25. P. R. Sharma, B. Zheng, S. K. Sharma, C. Zhan, R. Wang, S. R. Bhatia and B. S. Hsiao, *ACS Applied Nano Materials*, 2018, **1**, 3969-3980.
26. P. R. Sharma, A. Chattopadhyay, C. Zhan, S. K. Sharma, L. Geng and B. S. Hsiao, *Cellulose*, 2018, **25**, 1961-1973.
27. P. R. Sharma, R. Joshi, S. K. Sharma and B. S. Hsiao, *Biomacromolecules*, 2017, **18**, 2333-2342.
28. X. Xu, F. Liu, L. Jiang, J. Y. Zhu, D. Haagenson and D. P. Wiesenborn, *ACS Applied Materials & Interfaces*, 2013, **5**, 2999-3009.
29. T. Saito, S. Kimura, Y. Nishiyama and A. Isogai, *Biomacromolecules*, 2007, **8**, 2485-2491.
30. D. da Silva Perez, S. Montanari and M. R. Vignon, *Biomacromolecules*, 2003, **4**, 1417-1425.
31. A. Isogai, T. Saito and H. Fukuzumi, *Nanoscale*, 2011, **3**, 71-85.
32. C. B. Hollabaugh, L. H. Burt and A. P. Walsh, *Industrial & Engineering Chemistry*, 1945, **37**, 943-947.
33. N. V. Lukasheva, D. A. Tolmachev and M. Karttunen, *Physical Chemistry Chemical Physics*, 2019, **21**, 1067-1077.
34. S. Yang, Q. Xie, X. Liu, M. Wu, S. Wang and X. Song, *RSC Advances*, 2018, **8**, 3619-3625.
35. Z. Zhang, G. Sèbe, D. Rentsch, T. Zimmermann and P. Tingaut, *Chemistry of Materials*, 2014, **26**, 2659-2668.
36. M. Kaushik and A. Moores, *Green Chemistry*, 2016, **18**, 622-637.
37. K. Kanomata, N. Fukuda, T. Miyata, P. Y. Lam, T. Takano, Y. Tobimatsu and T. Kitaoka, *ACS Sustainable Chemistry & Engineering*, 2020, **8**, 1185-1194.
38. S. Hu, F. Jiang and Y.-L. Hsieh, *ACS Sustainable Chemistry & Engineering*, 2015, **3**, 2566-2574.
39. H. Golmohammadi, E. Morales-Narváez, T. Naghdi and A. Merkoçi, *Chemistry of Materials*, 2017, **29**, 5426-5446.
40. D. Trache, A. F. Tarchoun, M. Derradji, T. S. Hamidon, N. Masruchin, N. Brosse and M. H. Hussin, 2020, **8**.
41. N. Mahfoudhi and S. Boufi, *Cellulose*, 2017, **24**, 1171-1197.
42. J. Herrera-Morales, K. Morales, D. Ramos, E. O. Ortiz-Quiles, J. M. López-Encarnación and E. Nicolau, *ACS Omega*, 2017, **2**, 7714-7722.
43. Z. Karim, M. Hakalahti, T. Tammelin and A. P. Mathew, *RSC Advances*, 2017, **7**, 5232-5241.

44. P. R. Sharma and A. J. Varma, *Carbohydrate Polymers*, 2014, **114**, 339-343.
45. P. R. Sharma and A. J. Varma, *Chemical Communications*, 2013, **49**, 8818-8820.
46. P. R. Sharma, S. Kamble, D. Sarkar, A. Anand and A. J. Varma, *International Journal of Biological Macromolecules*, 2016, **87**, 460-465.
47. P. R. Sharma, P. R. Rajamohanan and A. J. Varma, *Carbohydrate Polymers*, 2014, **113**, 615-623.
48. P. R. Sharma and A. J. Varma, *Carbohydrate Polymers*, 2014, **104**, 135-142.
49. R. Das, T. Lindström, P. R. Sharma, K. Chi and B. S. Hsiao, *Chemical Reviews*, 2022, **122**, 8936-9031.
50. W. Chen, H. Yu, S.-Y. Lee, T. Wei, J. Li and Z. Fan, *Chemical Society Reviews*, 2018, **47**, 2837-2872.
51. R. Mangayil, S. Rajala, A. Pammo, E. Sarlin, J. Luo, V. Santala, M. Karp and S. Tuukkanen, *ACS Applied Materials & Interfaces*, 2017, **9**, 19048-19056.
52. X. Xu, R. Li, C. Tang, H. Wang, X. Zhuang, Y. Liu, W. Kang and L. Shi, *Carbohydrate Polymers*, 2018, **184**, 299-306.
53. Z. Cai, R. Li, X. Xu, G. Sun, X. Zhuang, Y. Liu and B. Cheng, *Polymer*, 2018, **156**, 179-185.
54. X. Hou, Z. Liu, Y. Wei, Q. Zhao, J. Dong, B. Liu, Z. Sun, T. Shi, M. Zhang and W. Hu, *Solid State Ionics*, 2017, **311**, 31-40.
55. C. Ni, H. Wang, Q. Zhao, B. Liu, Z. Sun, M. Zhang, W. Hu and L. Liang, *Solid State Ionics*, 2018, **323**, 5-15.
56. G. Jiang, J. Qiao and F. Hong, *International Journal of Hydrogen Energy*, 2012, **37**, 9182-9192.
57. S. Banerjee and D. E. Curtin, *Journal of Fluorine Chemistry*, 2004, **125**, 1211-1216.
58. H. Fukuzumi, S. Fujisawa, T. Saito and A. Isogai, *Biomacromolecules*, 2013, **14**, 1705-1709.
59. C. Vilela, A. J. D. Silvestre, F. M. L. Figueiredo and C. S. R. Freire, *Journal of Materials Chemistry A*, 2019, **7**, 20045-20074.
60. A. R. Kim, M. Vinothkannan, K. H. Lee, J. Y. Chu, B.-H. Park, M.-K. Han and D. J. Yoo, *International Journal of Energy Research*, 2022, **46**, 4835-4851.
61. C. Karthikeyan, Y. Sathishkumar, Y. S. Lee, A. R. Kim, D. J. Yoo and G. G. kumar, *Journal of Nanoscience and Nanotechnology*, 2017, **17**, 558-563.
62. A. R. Kim, J. C. Gabunada and D. J. Yoo, *Colloid and Polymer Science*, 2018, **296**, 1891-1903.
63. L. Liu, Z. Li and Q. Che, *ACS Applied Nano Materials*, 2019, **2**, 2160-2168.
64. T. D. O. Gadim, F. J. A. Loureiro, C. Vilela, N. Rosero-Navarro, A. J. D. Silvestre, C. S. R. Freire and F. M. L. Figueiredo, *Electrochimica Acta*, 2017, **233**, 52-61.
65. M. M. Hasani-Sadrabadi, E. Dashtimoghadam, R. Nasseri, A. Karkhaneh, F. S. Majedi, N. Mokarram, P. Renaud and K. I. Jacob, *Journal of Materials Chemistry A*, 2014, **2**, 11334-11340.
66. J. Tritt-Goc, I. Jankowska, K. Pogorzelec-Glaser, R. Pankiewicz and P. Ławniczak, *Cellulose*, 2018, **25**, 281-291.
67. C. Zhan, P. R. Sharma, L. Geng, S. K. Sharma, R. Wang, R. Joshi and B. S. Hsiao, *Science China Technological Sciences*, 2019, **62**, 971-981.
68. P. R. Sharma, A. Chattopadhyay, S. K. Sharma and B. S. Hsiao, *Industrial & Engineering Chemistry Research*, 2017, **56**, 13885-13893.
69. D. Wang, H. Yu, X. Fan, J. Gu, S. Ye, J. Yao and Q. Ni, *ACS Applied Materials & Interfaces*, 2018, **10**, 20755-20766.
70. Q. Yang, T. Saito, L. A. Berglund and A. Isogai, *Nanoscale*, 2015, **7**, 17957-17963.
71. L. C. A. Barbosa, C. R. A. Maltha, A. J. Demuner, C. M. Cazal, E. L. Reis and J. L. Colodette, *2013*, 2013, **8**, 12 %J BioResources.
72. S. Fujisawa, Y. Okita, H. Fukuzumi, T. Saito and A. Isogai, *Carbohydrate Polymers*, 2011, **84**, 579-583.
73. J. Zhang, H. Li and J. Zhang, *ECS Transactions*, 2019, **19**, 65-76.
74. P. Choi, N. H. Jalani and R. Datta, *Journal of The Electrochemical Society*, 2005, **152**, E123.